# Experimental Results from a Grazing Incidence X-ray Interferometer

Marshall Joy[1], Ann Shipley[2], Webster Cash[2],
James Carter[1], David Zissa[1], & Manfred Cuntz[3]

[1]NASA/Marshall Space Flight Center, Huntsville, AL 35812
[2]Center for Astrophysics and Space Astronomy, Univ. of Colorado, Boulder, CO 80303
[3]Center for Space Plasma and Aeronomic Research, Univ. of Ala., Huntsville, AL 35899

## Abstract

A prototype grazing incidence interferometer has been built and tested at EUV and X-ray wavelengths using a 120 meter long vacuum test facility at Marshall Space Flight Center. We describe the design and construction of the interferometer, the EUV and x-ray sources and detector systems, and compare the interferometric fringe measurements with theoretical predictions.

Keywords: X-rays, Interferometry, X-ray Astronomy, Grazing Incidence X-ray Optics

## I. Introduction

An x-ray interferometer in space has the potential to provide the single largest leap in imaging improvement ever attained. A mere 1 meter baseline can resolve 100 micro-arcseconds, a full factor of 1000 higher than the Hubble Space Telescope, and more than $10^6$ times higher than the Chandra X-ray Observatory. An essential step in establishing the viability of astronomical x-ray interferometry is the demonstration of a practical x-ray interferometer. We have now built and successfully tested an interferometer of this class; in this paper we describe the experiment and present the test results obtained at Extreme Ultraviolet (EUV) and x-ray wavelengths.

## II. Experimental Setup

The interferometer is of the simple four flat mirror design shown schematically in Figure 1. Tests were performed in a 120 meter long vacuum facility at the Marshall Space Flight Center. Compact x-ray and EUV sources were used to generate high energy photons, which then passed through a variable-width slit and then entered the interferometer located 16 meters down the vacuum pipe. The entrance aperture on the interferometer consisted of two parallel slits which ensured that the two primary mirrors were illuminated, but that none of the direct beam could enter the interferometer without reflecting off the optics.

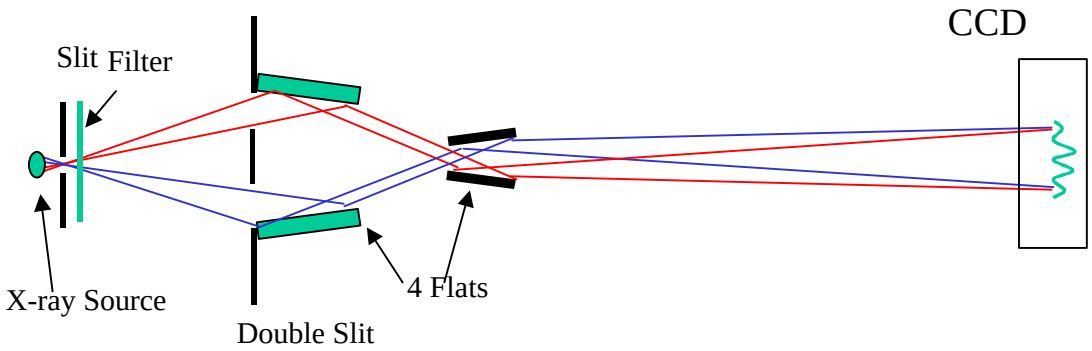


Fig. 1: Schematic of the interferometer used to create x-ray fringes.

The primary mirrors were 50mm dia. optical flats, set at 0.25 degrees to the incoming beam. Each was mounted in a precision manipulator that allowed fine rotational and translation adjustment from outside the vacuum tank as shown in Figure 2. The primary mirrors were separated by ~0.7 mm. The primary mirrors created reflected wavefronts that crossed and were then directed to the secondary mirrors, which were 17 mm away. The secondary mirrors were also 50mm dia. optical flats mounted on precision manipulators, and were set ~0.5 mm apart. The wavefronts, when they emerged from the secondary mirrors, were very nearly parallel. The wavefronts then traveled 100 meters down the vacuum pipe to the detector, where they were superimposed. Tests in both the EUV and x-ray spectral regions were performed, as described below.

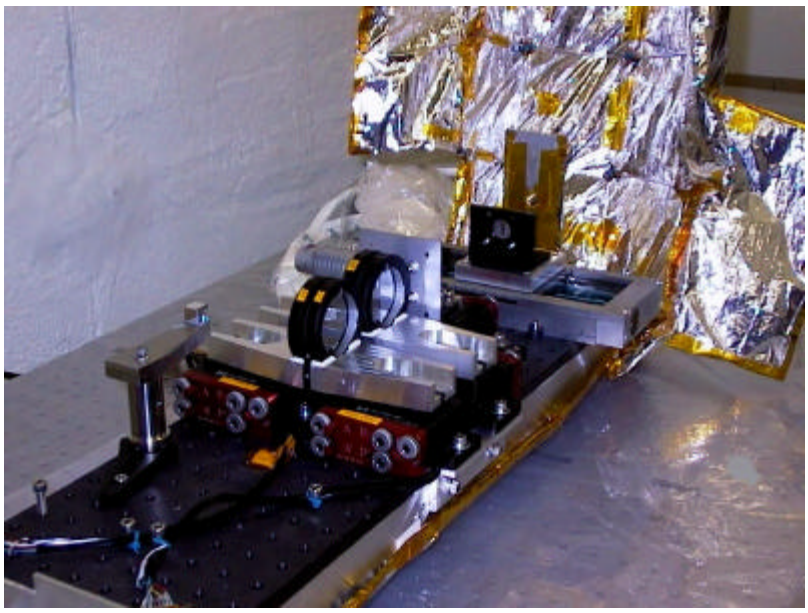

Figure 2: Photograph of the interferometer, consisting of a double-slit assembly and four flat mirrors mounted on precision manipulators.

*(a) EUV Results*

In July 1999 we used the facility at Marshall Space Flight Center to investigate performance in the Extreme Ultraviolet. For this wavelength range we used a micro-channel plate detector (Lampton, Siegmund, & Raffanti 1987). The photon source was a

hollow cathode discharge source (Paresce, Kumar, & Bowyer 1971) that creates very bright emission lines from noble gasses. We used a 0.15 μm thick aluminum filter to isolate the EUV portion of the spectrum and a 200 μm wide entrance slit. In Figure 3 we show the results. The signal amplitude was large, and the fringes spacing was also large because the whole system had been optimized for shorter wavelength x-rays.

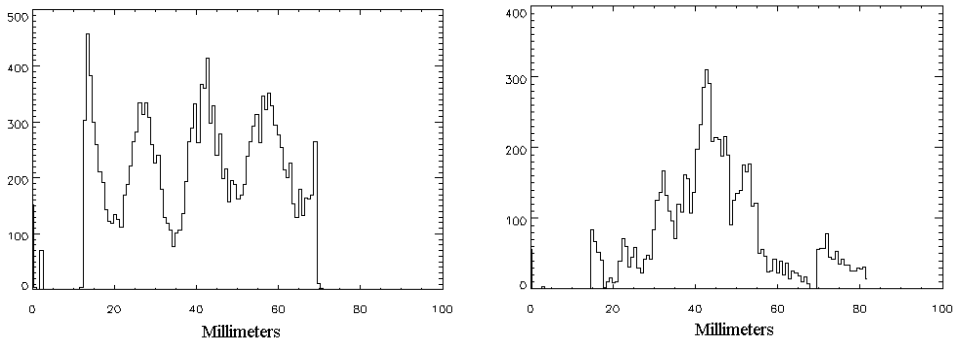


Figure 3: Interference fringes recorded in the extreme ultraviolet. (a) Fringes from neutral and singly ionized argon (92.0-106.7 nm). (b) Fringes from ionized helium (30.4 nm).

To the left in fig. 3 we show a profile of the fringes generated when argon was used in the source. The emission was from the resonance lines of neutral and singly ionized argon (ArI 104.8, 106.7 nm, and ArII 92.0, 93.2 nm). In the fringes from ionized helium (30.4 nm) on the right in fig. 3, we find a central fringe where there is zero optical pathlength difference, plus the fringes at one and two wavelengths of path difference on each side.

We performed the experiment of placing a block across the entrance to one of the two channels of the interferometer. We found that the signal dropped a factor of two, and that the fringes disappeared as expected, confirming that we were, in fact, seeing interference from the wavefront division into the two channels of the interferometer.

*(b) X-ray Results*

For demonstration of the interferometer in the x-ray we used a Manson Model 5 electron impact source with a magnesium target and 2 micron aluminum filter to create a beam that consists mostly of the Mg K photons (E=1.25keV). The x-ray beam was passed through a 5 μm wide slit and a thin Aluminum filter, and was then directed onto the interferometer. The x-rays were detected using a solid state CCD imaging detector with 18 micron pixels. A Loral 2048x2048 CCD was used, mounted in an Infrared Laboratories LN2-cooled cryostat which regulated the temperature of the CCD at ~ -80 C to suppress thermal dark current noise. The CCD system is interfaced via an Sbus controller to an Sun Sparcstation 5 for instrument control and data acquisition. When the system was turned on, each of the two beams created a vertical stripe of illumination on the CCD about a millimeter wide. The final step was to fine adjust the angles of the secondary mirrors so that the two stripes fell on top of each other at the CCD. Figure 4 shows two images from the CCD with the stripes of illumination clearly visible.

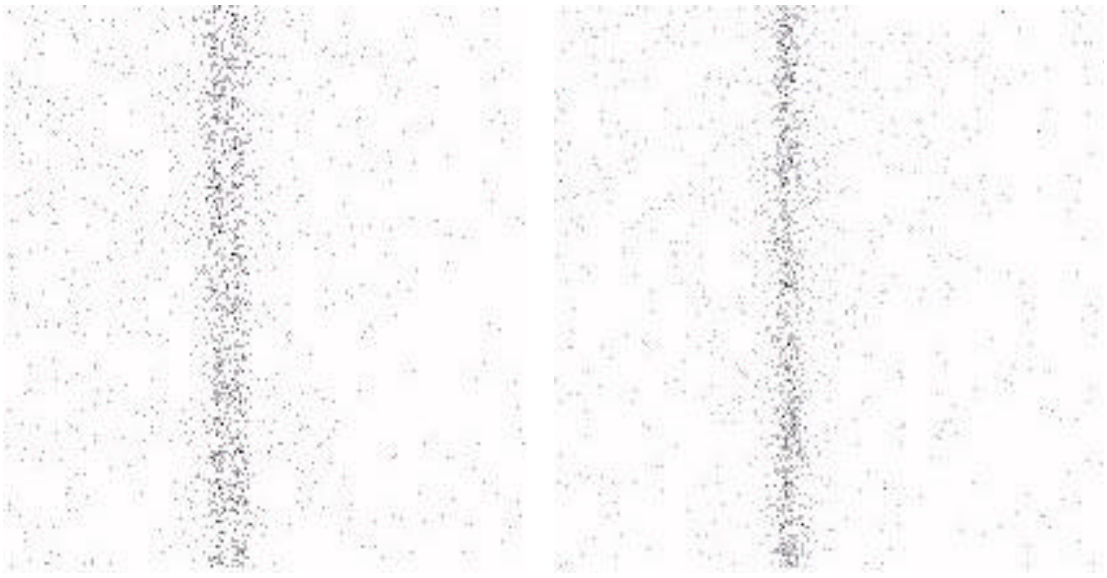

Figure 4: X-ray image taken with CCD imager. (a) The the two stripes on the left are from x-rays transmitted through the two sides of the grazing incidence interferometer, and then projected through the 100 meter long vacuum pipe. (b) On the right, fine adjustments to the grazing incidence mirrors have been made to superimpose the x-ray beams; the x-ray interference fringes lie within the overlapping beams.

The x-ray events in the image were filtered to accept photons in the energy band 1.24±0.15 keV, and the image was rotated 0.5 to allow for the slight angular misalignment between the fringes and the vertical axis of the CCD. The counts were then gathered into a histogram of events across the horizontal direction (Figure 5). A two bin boxcar smooth has been run across the data to suppress the Poisson noise. The overall appearance of the fringes is similar to those accumulated in the extreme ultraviolet. The main difference is that the fringe spacing is much smaller, as is to be expected at x-ray wavelengths.

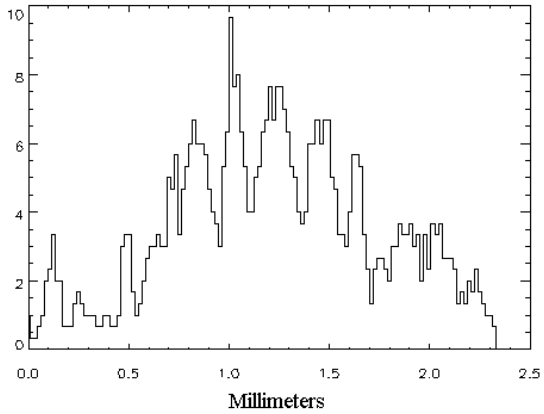


Figure 5: Histogram of events on the CCD with the two x-ray beams superimposed. The image was rotated half a degree and then binned. A two-bin boxcar smooth was run over the histogram to suppress Poisson noise. Fringes similar to those recorded in the EUV are clearly visible.

*(c) Comparison of x-ray data and theoretical predictions*

The fringe spacing predicted for a grazing incidence mirror system is $s=\lambda L/d$, where $\lambda$ is the x-ray wavelength, d is the separation of the mirrors, and L is the distance between the mirrors and the image plane (Shipley et al. 1999). The predicted spacing, s~0.2 mm, is in agreement with the data presented in fig. 5.

To first order, the theoretically predicted fringe pattern for our experimental geometry can be found by numerically superimposing a series of partial wave amplitudes,

$$A = \sum_j e^{-i(\omega t - kx_j)}$$

where $\omega$ is the frequency, t is the time, k is the wave number, and $x_j$ is the distance; the intensity distribution is obtained from the square of the amplitude. The fringe intensity simulations shown in Fig. 6 below correspond to a superposition of partial waves with 50% of the flux in the Mg K$\alpha$ line and 50% in the underlying x-ray continuum; the partial wave analysis also incorporates random phase errors with standard deviations of 0.002, 0.005, and 0.01 wavelengths. The simulations are in qualitative agreement with the data presented in fig. 5. More detailed modelling of the fringe pattern of a grazing incidence x-ray interferometer is explored in section III below.

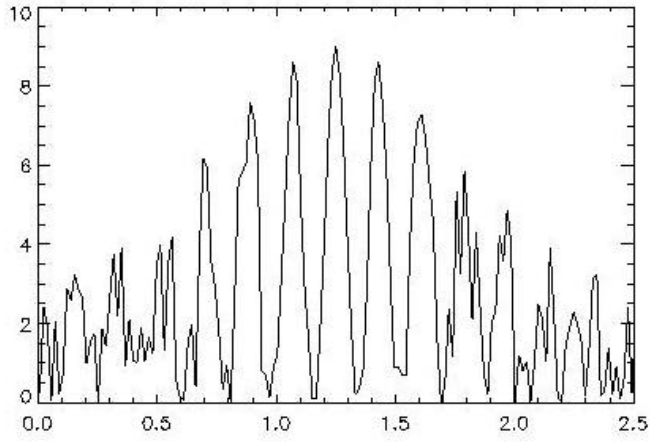


Fig. 6(a) Theoretical superposition of partial waves with RMS phase difference=0.002 wavelengths.

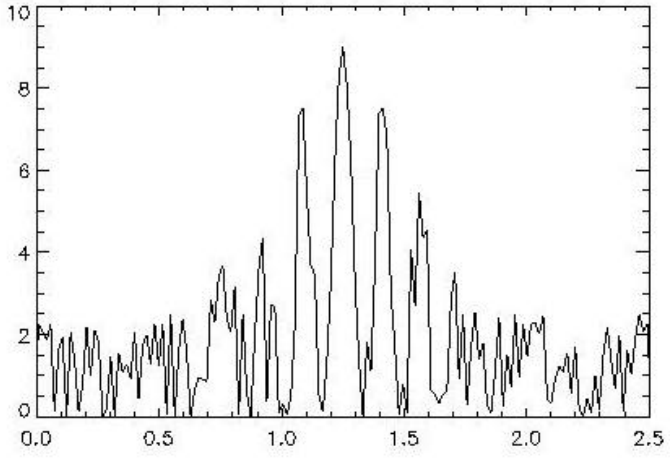


Fig. 6(b) Theoretical superposition of partial waves with RMS phase difference=0.005 wavelengths.

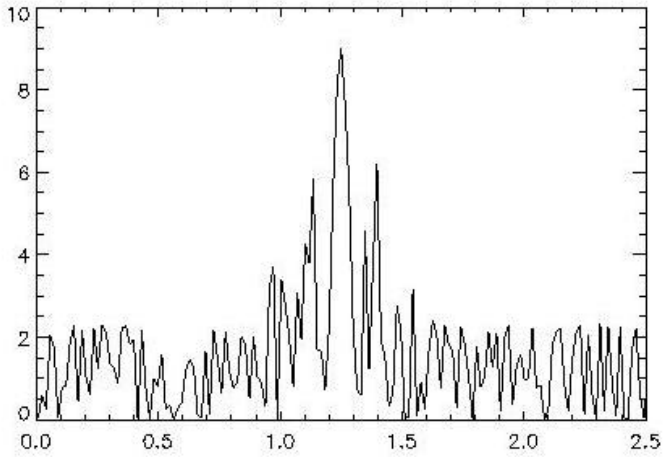


Fig. 6(c). Theoretical superposition of partial waves with RMS phase difference=0.01 wavelengths.

### III. Theoretical modelling of a next-generation x-ray interferometer

We have performed preliminary modelling of a next-generation x-ray interferometer, employing a set of four 6" long flat mirrors which are set at a grazing angle of 0.25 degrees. For this simulation, we assumed a parallel input x-ray beam and an interferometer-to-detector distance of 100 meters, which results in a beam convergence angle of 13.3 μrad. For an x-ray wavelength of 1 nm (1.24 keV), the fringe spacing should be ~75.2 μm, which corresponds to 19.1 bins in the plots. Our model made use of the optical design and analysis program CODE V from Optical Research Associates (ORA). The interferometer was ray-traced with non-sequential surfaces, and was then propagated to the image plane using the Fresnel beam propagation option. The results were checked against the results of the HEX3DE diffraction-based beam propagation program written by Martin E. Smithers of MSFC.

We present results from modelling two cases. The first model, illustrated in fig. 7, consists of perfectly flat mirrors. To determine the effect of mirror imperfections on the measured fringe pattern, we obtained a highly polished 6" flat (approximately $\lambda_{6328Å}/12$ RMS surface figure) and measured the actual deformations of the mirror surface using a Zygo interferometer, and then applied these measured deformations to one of the mirror surfaces in our simulated interferometer. The predicted fringe pattern for this second case is shown in fig. 8. The effect of mirror imperfections at the $\lambda_{6328Å}/12$ level is clearly evident in the fringe pattern; this modelling capability will be used to specify the mirror figure specifications that will be necessary to obtain the required interferometric imaging quality.

### Acknowledgements

The authors wish to thank the following individuals who made invaluable contributions to the experimental effort: J. Bixler, K. Doty, D. Goodman, K. Herren, T. Kester, J. Kolodziejczak, M. Weisskopf, and G. Zirnstein. This work was supported by NASA grants NAG5-5020 and 344-03-01-10.

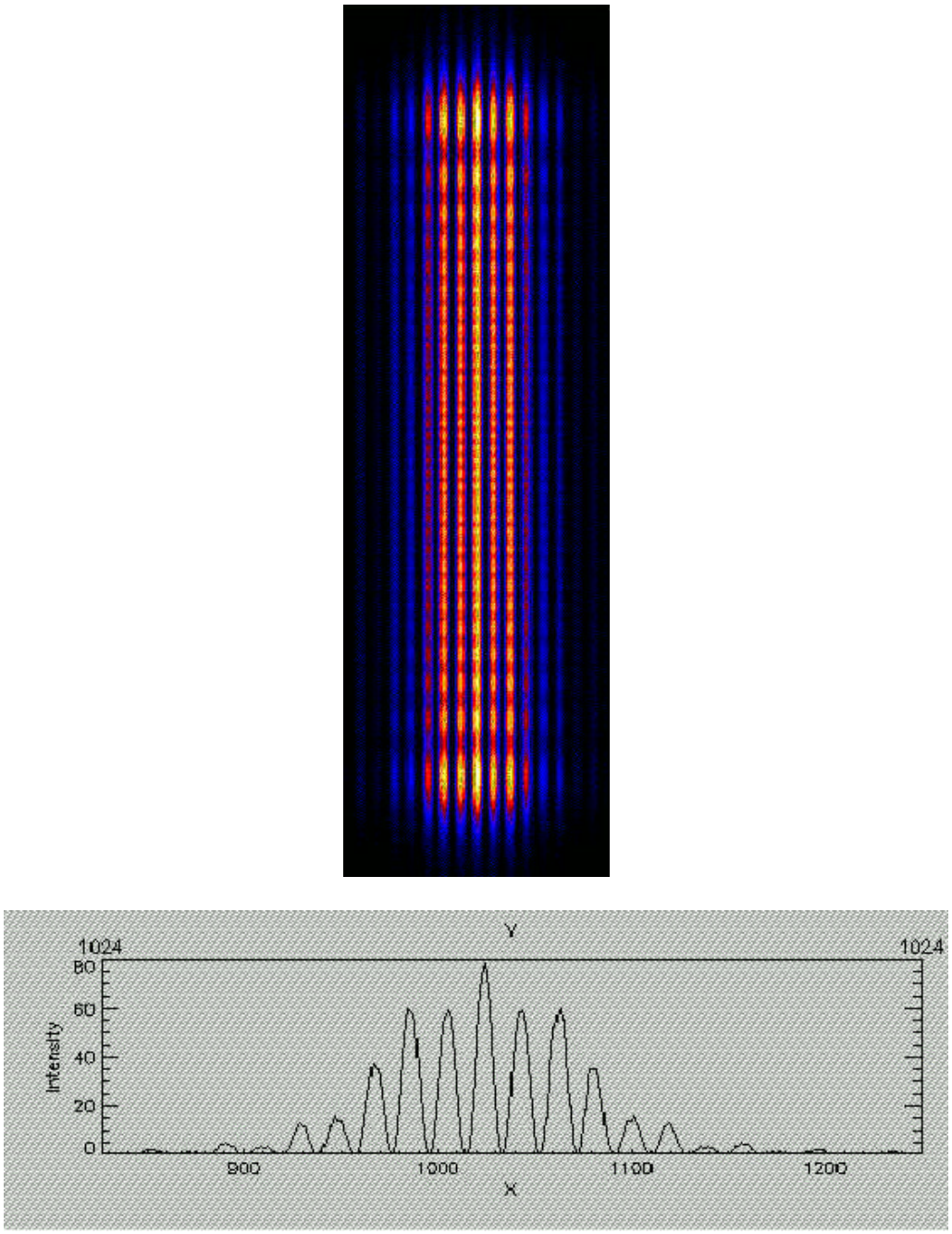


Fig. 7. Predicted performance of an x-ray interferometer with perfectly flat 6" long grazing incidence mirrors. (a) two-dimensional fringe pattern for 1 nm (1.24 keV) x-rays; (b) one-dimensional slice through the center of the fringe pattern. For an x-ray wavelength of 1 nm (1.24 keV), the fringe spacing should be ~75.2 μm, which corresponds to 19.1 bins in the plot.

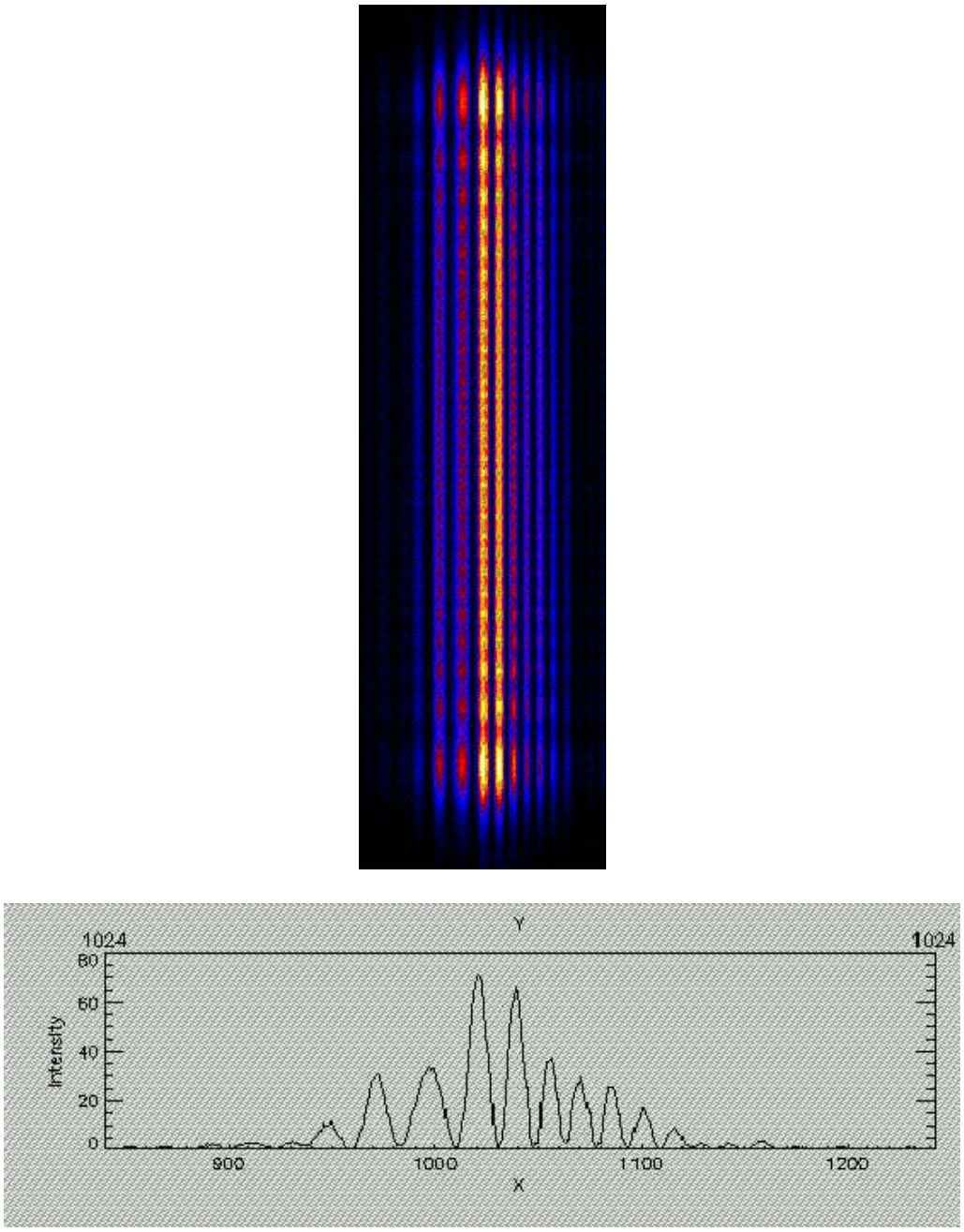


Fig. 8. Predicted performance of an x-ray interferometer which includes an imperfect mirror with $\lambda_{6328Å}/12$ RMS surface figure. (a) two-dimensional fringe pattern for 1 nm (1.24 keV) x-rays; (b) one-dimensional slice through the center of the fringe pattern.

## References

M. Lampton, O. Siegmund, and R. Raffanti, 1987, *Rev. Sci. Inst.*, **58**, 2298.
F. Paresce, S. Kumar, and C. S. Bowyer, 1971, *App. Opt.*, **10**, 1904.
A. Shipley, W. Cash, S. Osterman, M. Joy, and J. Carter, 1999, Proc. SPIE, **3786**, 291.